Heat release rate markers for highly-stretched premixed CH_4/air and CH_4/H_2/air flames

Xinyi Chen[1], Yiqing Wang[1], Thorsten Zirwes[2,3], Feichi Zhang[3], Henning Bockhorn[3], Zheng Chen[1,*]

[1] SKLTCS, CAPT, BIC-ESAT, College of Engineering, Peking University, Beijing 100871, China

[2] Steinbuch Centre for Computing, Karlsruhe Institute of Technology Hermann-von-Helmholtz-Platz 1, 76344, Eggenstein-Leopoldshafen, Germany

[3] Engler-Bunte-Institute, Chair of Combustion Technology, Karlsruhe Institute of Technology, Engler-Bunte-Ring 1, 76131, Karlsruhe, Germany

Abstract

Accurate quantification of heat release rate (HRR) profiles is useful for identifying important combustion processes in practical engines. This study aims to show whether the conventional HRR markers can still be used for highly-stretched premixed methane/air flames without and with hydrogen addition. The correlation of formaldehyde-based molar concentrations, $[H][CH_2O]$ and $[OH][CH_2O]$, with HRR is numerically studied for highly-stretched premixed CH_4/air and CH_4/H_2/air flames. Two types of premixed flames are considered: the spherically expanding flame (SEF) starting from highly positively stretched ignition kernel, and Bunsen flame with high negative stretch rate at the flame tip. It is found that both $[H][CH_2O]$ and $[OH][CH_2O]$ can qualitatively describe the spatial distribution of HRR profiles in these two types of flames. Compared to $[H][CH_2O]$, $[OH][CH_2O]$ is slightly better since it has a higher correlation coefficient and weaker sensitivity to the stoichiometry. However, during the ignition-influenced regime of SEFs, the magnitude of HRR cannot be accurately correlated by the concentrations of CH_2O, OH and H. Besides, hydrogen addition does not change the good spatial reconstruction qualities of these two HRR markers when its volume fraction in methane/hydrogen binary fuel blends is below 70%. The present results demonstrate that the conventional HRR markers, $[OH][CH_2O]$ and $[H][CH_2O]$, can be used to quantify the shape of HRR profiles even for highly-stretched premixed flames with small amount of hydrogen addition. Nevertheless, the magnitude of HRR cannot be accurately correlated by these two HRR markers for highly-stretched ignition kernel and hydrogen-dominated binary fuel blends.

Keywords: Heat release rate marker, stretch rate, methane, hydrogen, premixed flame

* Corresponding author. E-mail: cz@pku.edu.cn

1. Introduction

Heat release rate (HRR) is a fundamental physicochemical property of the combustion process. The magnitude of HRR characterizes the energetic outcome of the combustion process, and the spatial distribution of HRR is useful to represent the flame front.[1] Therefore, accurate quantification of HRR profiles is essential to the proper evaluation of combustion performance in practical engines.

Unfortunately, direct experimental measurement of HRR is not practical yet, since it requires simultaneous measurement of temperature and full-spectrum species concentrations.[2] An alternative, indirect approach is to measure the concentrations of certain markers or indicators which correlate well with the HRR over the relevant range of flame parameters. Generally, both chemiluminescence and laser-induced fluorescence (LIF) measurements have been used in the literature to track the HRR profile across the flame front. The chemiluminescence measurement is based on the natural visible emission from excited molecules such as CH*, OH* and CO_2*.[3] It measures the concentration of species produced in an excited electronic state far away from the equilibrium. In previous studies,[4-6] the chemiluminescence emission from CH* and/or OH* was reported to be good indicators of HRR. However, the chemiluminescence measurement is based on the total emission along the line of sight and is not spatially resolved,[3] especially in complex flame topologies such as turbulent flames.

As an alternative, the LIF technique, which is spatially resolved and can be extended to a planar imaging geometry (PLIF), performs as a promising method to measure concentrations of HRR indicators. The LIF measurement is a null background absorption-based technique. It requires sophisticated lasers to excite target species and then sample the ground electronic state of the specific species. The formyl radical, HCO, was first found to have a strong correlation with HRR for laminar methane/air flames by Najm and his co-workers.[3, 7] It was found that

HCO reactions are not the primary source of heat release in the flames and HCO is simply a good rate-measure of the forward progress of hydrocarbon conversion to H_2O and CO_2. However, the fluorescence signal from HCO is too weak due to its low concentration. To circumvent this difficulty, Paul and Najm[8] proposed a pixel-by-pixel product of CH_2O and OH PLIF images to track the local HRR. This method is based on the assumption that HCO forms from the elementary reaction $OH+CH_2O=HCO+H_2O$. Compared to HCO, the fluorescence signals from OH and CH_2O PLIF are relatively more intense and can be quantitatively measured. According to their results, the product of CH_2O and OH concentrations was shown to be a reliable indicator for HRR distribution. Since then, the combined molar concentration $[OH][CH_2O]$ has been widely adopted in numerous studies for different flame types (e.g. premixed[4, 9, 10] and non-premixed flames[11], auto-ignition assisted[1] and conventional freely propagating flames[2]), different flame configurations (e.g. Bunsen flames[9], spray flames[1, 12]), different flow conditions (e.g. counterflow flames[13], jet flames[14], turbulent flames[4, 9]), and different fuels (e.g. complex hydrocarbons[1, 12] and multicomponent fuels[15]). Recently, it has been noticed that HCO forms also through the reaction $H+CH_2O=HCO+H_2$.[15] The performance of $[H][CH_2O]$ was then compared with $[OH][CH_2O]$ by Mulla et al.[2] for methane/air flames with a wide range of equivalence ratio. It was shown that $[H][CH_2O]$ is also a reliable indicator for HRR and it is less sensitive to the stoichiometry variation. Currently, the two formaldehyde-based concentration products $[H][CH_2O]$ and $[OH][CH_2O]$ are the most commonly used indicators for HRR profiles.

In practical turbulent combustion processes, the local flame front might be highly curved and stretched.[16-18] For example, in spark ignition engines the self-sustained propagation flame develops from an ignition kernel which is affected by high positive stretch rate, and in fuel-lean turbulent combustion there is local flame quenching and re-ignition processes caused by high strain/stretch rate. Therefore, it is necessary to know whether the conventional HRR

markers, [H][CH_2O] and [OH][CH_2O], can still be used for highly-stretched premixed flames. The first objective of this study is hence to assess the performance of these two HRR markers for highly-stretched premixed flames. Two types of premixed flames are considered: the spherically expanding flames (SEF) starting from a highly positively stretched ignition kernel, and the Bunsen flames with high negative stretch rate at the flame tip.

Recently, there is an increased interest in developing hydrogen-based combustion systems. However, there are difficulties in hydrogen application and storage considering its broad flammability range, high laminar flame speed, low ignition energy, and low volumetric energy density.[19] Therefore, a more reasonable way is to use hydrogen as an additive to traditional fossil fuels.[20] For example, it was demonstrated that promising performance can be achieved by using methane/hydrogen binary fuel blends in internal combustion engines.[21] In the literature, there are many studies on the fundamental combustion properties of hydrogen/hydrocarbon binary fuel blends.[20, 22-27] However, to our knowledge, the HRR markers have not been studied for premixed flames in hydrogen/hydrocarbon/air mixtures. Therefore, the second objective of this study is to assess the feasibility of formaldehyde-based correlations, [H][CH_2O] and [OH][CH_2O], for highly-stretched premixed flames in methane/air mixtures with hydrogen enrichment.

This paper is organized as follows. The numerical models and methods are provided in Section 2. In Section 3, the correlation between formaldehyde-based concentrations and HRR is evaluated in both positively-stretched SEF from ignition kernel and negatively-stretched Bunsen flames at the flame tips for CH_4/air and CH_4/H_2/air mixtures. The conclusions are summarized in Section 4.

2. Numerical models and methods

We consider laminar, stretched, premixed flames in CH_4/H_2/air mixtures. The unburned

mixture composition is specified according to $\phi[(1-a)CH_4+aH_2]+(2-1.5a)[O_2+3.76N_2]$ where ϕ is the equivalence ratio and a is the volume fraction of hydrogen in the methane/hydrogen binary fuel blends. The unburned mixtures are initially at T_0=298 K and P_0=1 atm. Fuel-lean (ϕ=0.7), stoichiometric (ϕ=1), and fuel-rich (ϕ=1.3) mixtures with 0~95% H_2 enrichment (i.e. a=0~0.95) are considered. Two types of stretched premixed flames are considered: one is SEF with positive stretch rate and the other is Bunsen flame with negative stretch rate. The numerical models and methods for these two flames are described below.

2.1 Spherically expanding flame

A SEF can be initiated from central spark ignition in a quiescent mixture, and it is popularly used in laminar flame speed measurement.[28-30] The SEF is exposed to positive stretch rate, which is inversely proportional to the flame radius. Therefore, the small ignition kernel is highly stretched. The initiation and propagation of SEFs are simulated using the in-house code A-SURF,[31, 32] which solves the conservation equations for multi-component, reactive flow using the finite volume method. ASURF has been successfully used in previous studies on ignition and flame propagation.[33-37] The details on numerical schemes and code validation can be found in references[31, 32] and thereby are not repeated here.

Due to the spherical symmetry of SEF, the simulations are one-dimensional in a spherical coordinate. The computational domain is $0 \leq r \leq 50$ cm with zero gradients of temperature and mass fractions enforced at both boundaries at r = 0 and r =50 cm. For flame radius less than 5 cm, the pressure rise is negligible. The homogenous mixture is initially static, and uniformly distributed over the computational domain. Similar to practical spark ignition process in engines, the mixture is centrally ignited through energy deposition given by the following source term in the energy equation[38] :

$$q_{ig}(r,t)=\begin{cases}\dfrac{E_{ig}}{\pi^{1.5}r_{ig}^{3}\tau_{ig}}\exp[-(\dfrac{r}{r_{ig}})^{2}] & if \quad t<\tau_{ig}\\ 0 & if \quad t\geq\tau_{ig}\end{cases} \tag{1}$$

where E_{ig} is the total input ignition energy, τ_{ig}=0.2 ms is the duration of energy deposition, and r_{ig}=0.2 mm is the radius of the energy deposited region. To accurately and efficiently resolve the propagating flame, locally adaptive mesh refinement is used and the reaction front is always covered by the finest mesh in the width of 8 μm which ensures grid convergence of the present simulation results. Since the mixtures considered here are far from the corresponding flammability limit, radiation heat loss has negligible effects on SEF[39-41] and thereby is not considered in present simulations.

2.2 Bunsen flame

A premixed Bunsen flame can be stabilized at the burner rim for a considerable range of the flow velocity and mixture composition.[42] The flame surface is curved by the strained flow, leading to a large proportion of flame front subjected to the negative stretch rate. In this study, 2D steady cylindrical Bunsen-type flames are simulated using the in-house solver,[43, 44] which is developed based on the open-source CFD framework OpenFOAM. In this solver, the finite volume method is used to solve the fully compressible conservation equations for multi-component reactive flows. Cantera[45] is incorporated for the calculation of reaction rates and transport coefficients. This code was used in recent studies on premixed flames.[46-48] More details on numerical schemes and code validation can be found in references.[43, 44]

The domain is 2D with rotational symmetry. All dimensions of the domain are set as multiples of the thickness and flame speed of the unstretched planar flame, similar to the settings in Zirwes et al.'s work. [49] The unburned mixture enters the domain at the inlet with a parabolic velocity profile given by the Poiseuille solution. For each equivalence ratio, the bulk velocity is adjusted so that the flame tip is far enough away from the inlet. The burned mixture

leaves the domain from the outlet, where zero gradients of velocity, temperature and mass fractions are enforced. The lateral boundaries are defined as slip wall with zero gradients. In simulations, the reaction zone is always covered by at least 20 cells so that the reaction zone can be adequately resolved. Similar configuration was also adopted by Zirwes et al.[49] (see Fig. 3 therein).

In the simulations of both Bunsen flames and SEFs, the detailed kinetic model for methane oxidation, GRI Mech 3.0,[50] is used and the mixture-averaged transport model is used for the diffusion velocity. It is noted that recently several kinetic models have been developed for methane and their performance in predicting premixed methane/air flames was assessed by Wang et al.[51] They found that at ambient conditions the results predicted by seven kinetic models are very close while larger discrepancy is observed for engine-relevant conditions.[51] Since this work considers premixed flames at normal temperature and pressure, GRI Mech 3.0 is used here, and the present conclusions are expected to be independent of the kinetic model used in simulations. If HRR under engine-relevant conditions is studied in future works, GRI Mech 3.0 should not be used.

2.3 Correlation coefficient

The correlation of species concentration with HRR can be quantified by different coefficients. We use the following correlation coefficient which was also used by Yin et al.[1]:

$$\rho(A,B) = \frac{1}{N-1}\sum_{i=1}^{N}\left(\frac{A_i-\mu_A}{\sigma_A}\right)\left(\frac{B_i-\mu_B}{\sigma_B}\right) \tag{2}$$

where A and B are the evaluated quantities. μ_i and σ_i are the mean and standard deviation, respectively. The linear correlation between HRR and its indicator/marker can be quantified by:

$$C(\nu) = \rho(Q,\nu) \tag{3}$$

where Q is the heat release rate and ν is the molar concentration of the individual or combined species.

In simulations, we only consider the HRR above 1% of its peak value, i.e., $Q>0.01Q_{max}$. A large number of samples are equidistantly extracted from HRR and species molar concentration profiles along the normal direction of the flame front so that a good estimation of correlation coefficient can be approached. Combined species molar concentration with a larger $C(v)$ has greater potential to be a reliable HRR indicator.

3. Results and discussion

3.1 Positively-stretched SEFs in CH_4/air mixtures

In this subsection, we assess the effect of stretch on the correlation between HRR and species concentrations for SEFs in CH_4/air mixtures without H_2 addition.

Figure 1 shows the flame propagation speed as a function of stretch rate for SEF in stoichiometric CH_4/air mixtures at two ignition energies, E_{ig} = 0.175 and 1 mJ. The flame radius/position, R_f, is defined as the location where the HRR is maximum. The flame propagation speed is defined as $S_b = \mathrm{d}R_f/\mathrm{d}t$, which represents the stretched flame speed relative to the burned gas. In SEF, the stretch rate is $K = 2U/R_f$ where $U=S_b$. It is seen that the ignition kernel has very high stretch rate at around 4000 s^{-1}. For low ignition energy of E_{ig} = 0.175 mJ, three regimes are observed: the spark-assisted ignition kernel propagation regime (line DC in Fig. 1), the unsteady flame transition regime (CB), and the normal flame propagation regime (BA). However, for relatively high ignition energy of E_{ig} = 1 mJ, only two regimes, FE and EA in Fig. 1, are observed. These regimes have been identified for different fuels and discussed in details in previous studies.[32, 33]

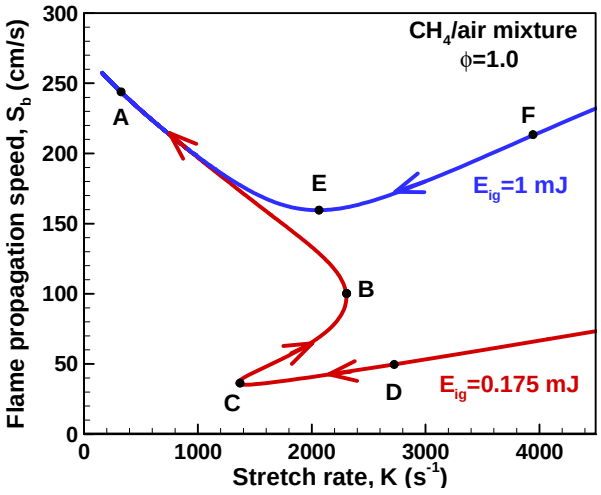

Figure 1. Change of the flame propagation speed with stretch rate during the ignition and propagation of SEF in a stoichiometric CH_4/air mixture with different ignition energies of E_{ig} = 0.175 and 1 mJ. The flame radius increases along the line in the direction marked by the arrows.

The profiles of HRR, [OH][CH_2O] and [H][CH_2O] are compared in Fig. 2 for points A-F marked in Fig. 1. All the quantities in Fig. 2 are normalized by their corresponding peak values in the unstretched, adiabatic, planar flame, which can be obtained from PREMIX.[52] The highly-stretched ignition kernel is mainly driven by the ignition energy deposition. Due to the excess enthalpy from the initial external energy addition, the stretched flame at point D corresponds to higher HRR and radical concentrations compared to the unstretched flame (e.g. the peak value of HRR is about 2.8 times of that in unstretched planar flame, and the peak value of [H][CH_2O] is about 1.9 times of that in unstretched planar flame). The trends in spatial distributions of [OH][CH_2O] and [H][CH_2O] agree well with the HRR profile. However, it is noted that the peak values of normalized [OH][CH_2O] and [H][CH_2O] are slightly lower than their corresponding normalized HRR peak. This indicates that [OH][CH_2O] and [H][CH_2O] can spatially describe the HRR distribution, but cannot accurately represent the magnitude of HRR when the flame is influenced by the ignition energy deposition.

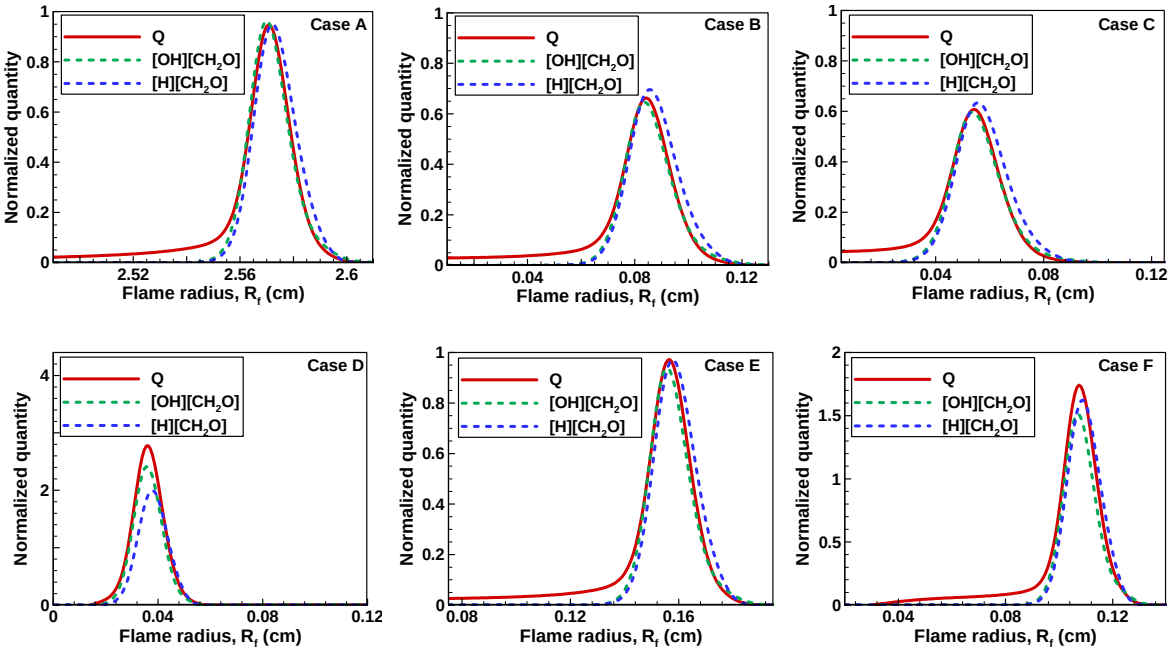

Figure 2. Normalized HRR and radical mole concentration profiles for cases A-F, which correspond to points A-F marked in Fig. 1.

After energy deposition, the reaction rates and ignition kernel propagation speed rapidly decay from point D to point C which has the lowest propagation speed and reactivity as shown in Fig. 1. Figure 2 shows that the peak values of the HRR, [OH][CH_2O] and [H][CH_2O] are only around 0.6 times of that in unstretched planar flame. Nevertheless, the trends and magnitudes in HRR, [OH][CH_2O] and [H][CH_2O] are in good agreement. From points C to B in Fig. 1, the spark-assisted ignition kernel evolves into a self-sustaining flame. Therefore, the flame B is mainly driven by chemical reaction and transport rather than deposited ignition energy. After the unsteady transition, the SEF propagates in a quasi-steady manner approaching zero stretch rate. In experiments, linear or nonlinear extrapolation is conducted in this regime to obtained the unstretched flame speed.[28] For stoichiometric CH_4/air mixture with positive Markstein length, the positive stretch rate imposed on SEF weakens the flame. Therefore, when SEF propagates from points B to A, the HRR and radical concentrations both increase as shown in Fig. 2. At point A, the [H][CH_2O] and [OH][CH_2O] profiles are in good agreement with the HRR profile. It is noted that at point A, the post oxidation zone after the main reaction zone

tends to be very long and the low HRR there is not well captured by either marker. This low HRR region is dominated by exothermic reactions such as $H+OH+M=H_2O+M$ and $OH+HO_2=O_2+H_2O$, which slowly approach the equilibrium state. These reactions do not involve the main reaction path leading to CO and CO_2 via HCO. Therefore, the low HRR is not well captured by HCO or either HRR markers.

Figure 2 shows that the profiles for point F with E_{ig} = 1 mJ are similar to those for point D with E_{ig} = 0.175 mJ. For both points F and D, the HRR and radical concentrations are enhanced by the excess enthalpy from energy deposition. Similar to point D, the peak values of normalized $[OH][CH_2O]$ and $[H][CH_2O]$ are also slightly lower than the peak value of the normalized HRR at point F. This suggests that the normalized $[OH][CH_2O]$ and $[H][CH_2O]$ are not suitable for the prediction of the magnitude of the normalized HRR during the initial ignition-influenced phase. Nevertheless, $[OH][CH_2O]$ and $[H][CH_2O]$ are still suitable markers for the spatial distribution of HRR. The above results indicate that the ignition energy can affect the initial ignition kernel development, while it has negligible effect on the spatial correlation between HRR and species molar concentrations.

Figures 3 and 4 show the scatter plots of the normalized HRR against normalized $[OH][CH_2O]$ and $[H][CH_2O]$ for SEFs in different regimes with different ignition energies. Similar to Fig. 2, all the quantities are normalized by their corresponding peak values in the unstretched, adiabatic, planar flame. For both ignition energies, $[OH][CH_2O]$ and $[H][CH_2O]$ show positive correlation with the HRR during the whole ignition and flame propagation processes. The red points (representing flames in regimes CD and EF) distribute dispersedly in the region with higher HRR, implying that the HRR markers have relatively poor performance in spark-assisted ignition kernel propagation regime due to the energy deposition effect. The blue points (representing flames in regime BC) and green points (representing flames in regimes AB and AE) show good linear correlation between HRR and its markers. Compared to

[H][CH_2O], [OH][CH_2O] has a slightly better linear correlation with the HRR. This was also observed for turbulent premixed CH_4/air flames simulated by Chi et al.[10]

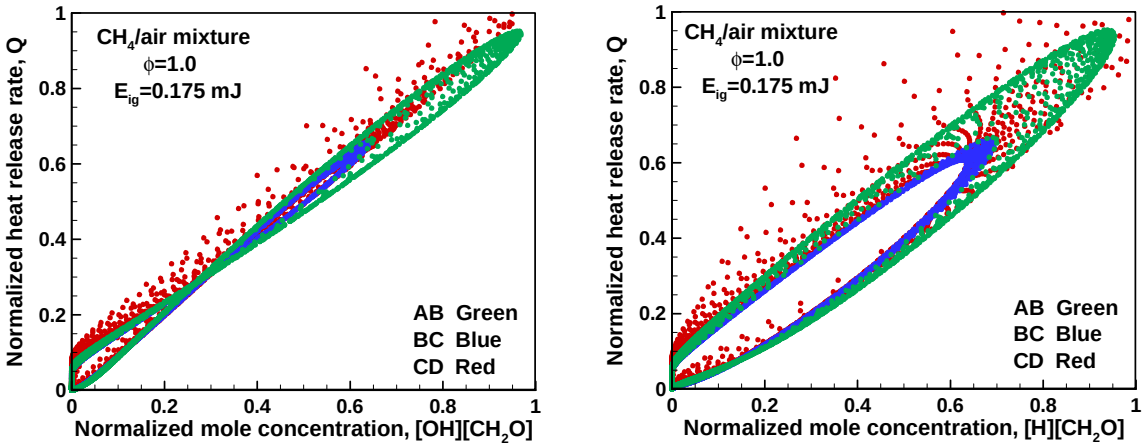

Figure 3. Scatter plots of normalized HRR against normalized [OH][CH_2O] and [H][CH_2O] for three regimes, AB, BC and CD, shown in Fig. 1 for E_{ig} = 0.175 mJ.

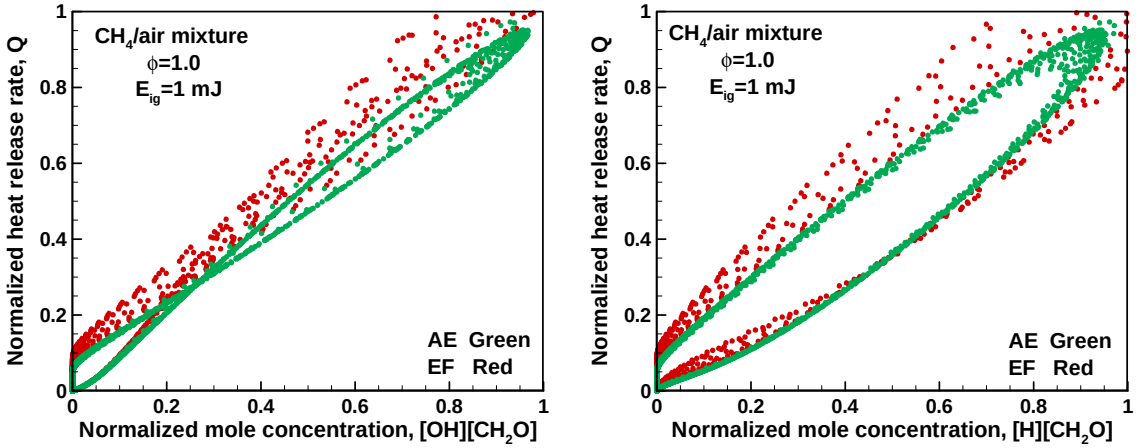

Figure 4. Scatter plots of normalized HRR against normalized [OH][CH_2O] and [H][CH_2O] for two regimes, AE and EF, shown in Fig. 1 for E_{ig} = 1.0 mJ.

For quantitative comparison, the correlation coefficients are plotted in Fig. 5. Consistent with the scatter plots in Fig. 4, the correlation coefficient for [OH][CH_2O] is higher than that for [H][CH_2O] for both ignition energies. For E_{ig} = 0.175 mJ, the correlation coefficient changes non-monotonically with the stretch rate, the trend of which is similar to the trend in the S_b-K plot in Fig. 1. For E_{ig} = 1.0 mJ, the correlation coefficient is shown to be insensitive to the

stretch rate. Overall, both [OH][CH_2O] and [H][CH_2O] exhibit good linear correlation with HRR during the ignition and propagation of the SEF.

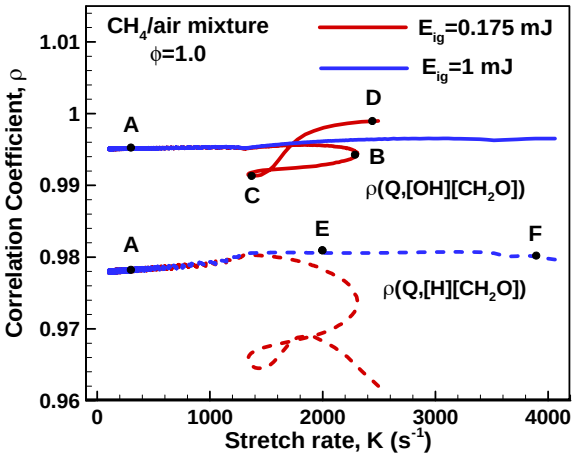

Figure 5. Change of the correlation coefficient with stretch rate during the ignition and propagation of SEF in a stoichiometric CH_4/air mixture with E_{ig} = 0.175 and 1.0 mJ. Points A-F are the same as those marked in Fig. 1.

Besides the stoichiometry case considered above, we also study fuel-lean (i.e. ϕ = 0.7) and fuel-rich (i.e. ϕ = 1.3) CH_4/air mixtures. The results are shown in Fig. 6. The trends of flame propagation speed and correlation coefficients are shown to be similar to those in Figs. 1 and 5. Figure 6(b) shows the correlation coefficients vary strongly with stoichiometry and stretch rate. Compared to [H][CH_2O], [OH][CH_2O] has a higher correlation coefficient rate and lower sensitivity to the stoichiometry variation. Furthermore, it is observed that the correlation coefficient for fuel-rich CH_4/air flame is much higher than that for fuel-lean case. Therefore, the combined-species markers are suitable for stoichiometric and fuel-rich mixtures, while extension of these marker to fuel-lean mixtures should be performed with caution.

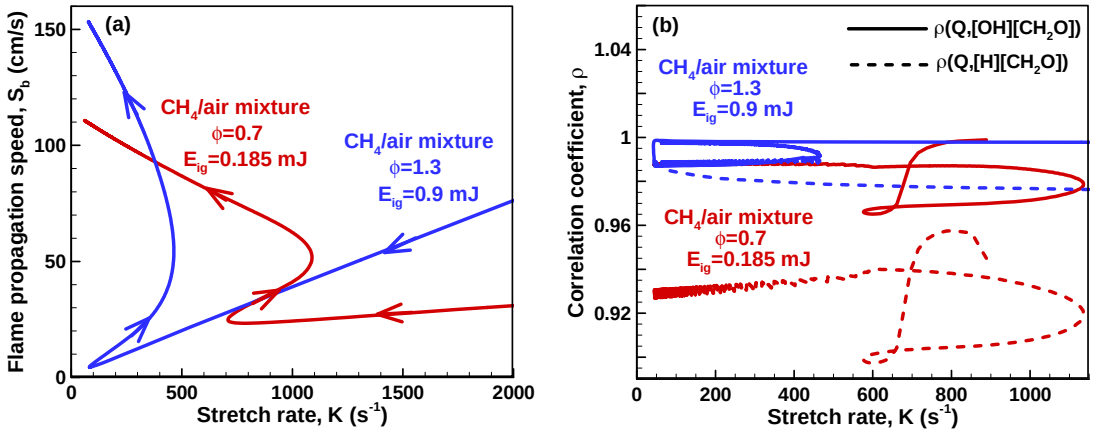

Figure 6. Change of (a) flame propagation speed and (b) correlation coefficients with stretch rate during the ignition and propagation of SEF in CH_4/air mixtures with ϕ = 0.7 and 1.3.

3.2 Positively-stretched SEFs in CH_4/H_2/air mixtures

In this subsection, CH_4/H_2/air mixtures are considered and the effects of H_2 enrichment on the correlation of HRR with species concentrations are assessed.

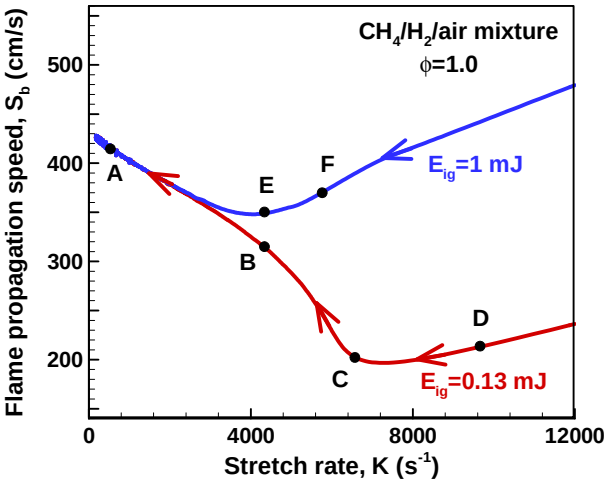

Figure 7. Change of the flame propagation speed with stretch rate during the ignition and propagation of SEF in a stoichiometric CH_4/H_2/air mixture with a=0.5 (i.e., CH_4:H_2=1:1) at different ignition energies of E_{ig} = 0.13 and 1 mJ.

Figure 7 shows the flame propagation process for 50% H_2 in the binary fuel blends. Compared to Fig. 1 for stoichiometric CH_4/air mixture without H_2 addition, Fig. 7 shows that H_2 addition greatly increases the flame propagation speed. Besides, the minimum ignition

energy is reduced from 0.175 mJ (see Fig. 1) to 0.13 mJ due to H_2 addition. Nevertheless, similar to Fig. 1, the trends for S_b-K curves are not affected by H_2 addition; three and two regimes are also observed respectively for relatively low and high ignition energies.

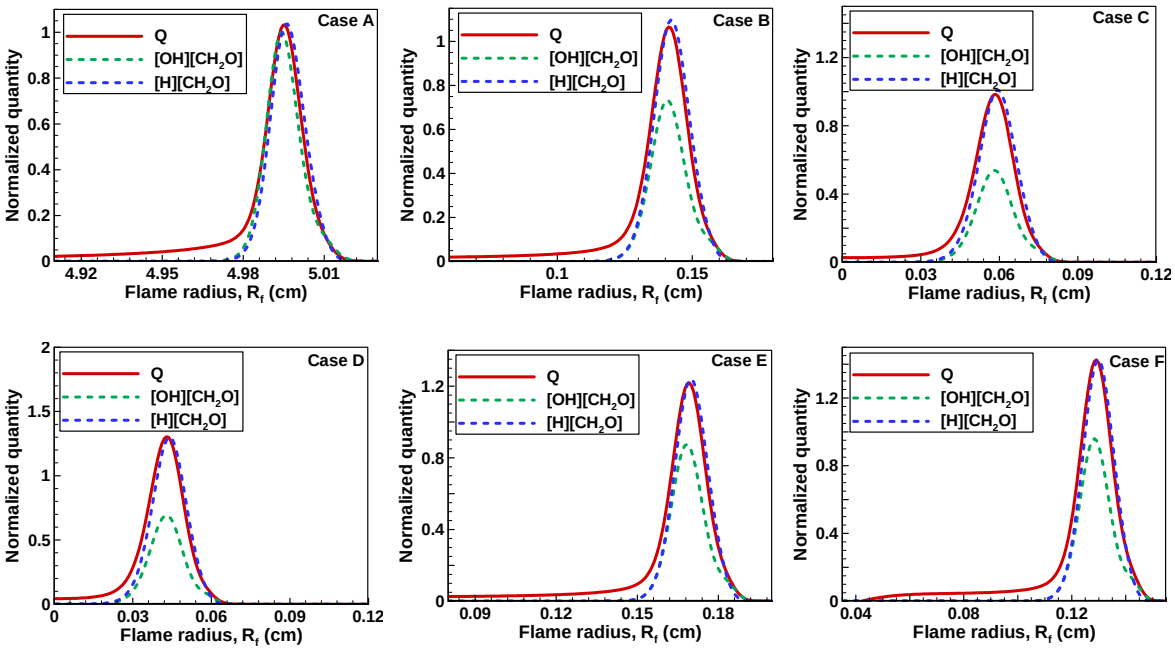

Figure 8. Normalized HRR and radical mole concentration profiles for cases A-F, which correspond to points A-F marked in Fig. 7.

Figure 8 plots the profiles of HRR, [OH][CH_2O] and [H][CH_2O] for points A-F marked in Fig. 7. Similar to Fig. 2 for CH_4/air without H_2 addition, the same qualitative conclusions can be drawn for CH_4/H_2/air stretched flames. The profiles are qualitatively similar at different stretch conditions and the spatial correlations of HRR with [OH][CH_2O] and [H][CH_2O] are independent of the stretch rate. One notable difference from results for CH_4/air is that the normalized peak value of [OH][CH_2O] is significantly lower than that of HRR during the ignition-influenced phase (see cases B-F in Fig. 8) for CH_4/H_2/air. This is because the H_2 addition increases HRR and produces a large amount of H radical during the initial ignition-influenced phase. This implies that [OH][CH_2O] is unsuitable to quantify the magnitude of HRR for high-stretched ignition kernel.

The correlations between HRR and [OH][CH_2O] and between HRR and [H][CH_2O] at

different ignition energies are shown in Figs. 9 and 10. During the ignition-influenced phase (i.e. regimes BC and CD in Fig. 9 and EF in Fig. 10), [OH][CH_2O] shows a poor linear correlation with the scatters far away from the diagonal. This is consistent with results in Fig. 8, where the peak of normalized [OH][CH_2O] is much lower than that of the normalized HRR. When the ignition kernel evolves into a self-sustaining flame (i.e. regime AB in Fig. 9 and regime AE in Fig. 10), the scatters lie very close to the diagonal. Compared to [OH][CH_2O], [H][CH_2O] shows a much better proportionality throughout the whole ignition and flame propagation processes. Nevertheless, in the normal flame propagation regime unaffected by ignition, [OH][CH_2O] is still a good HRR marker.

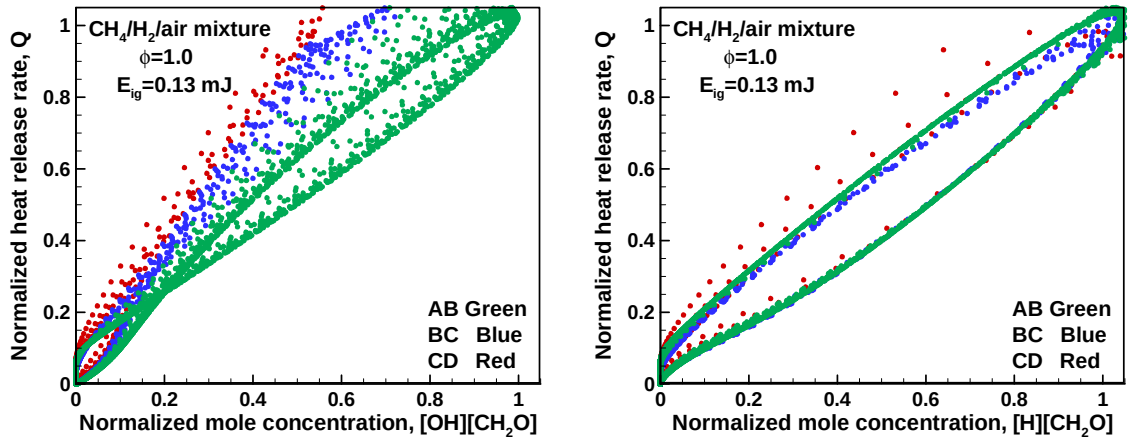

Figure 9. Scatter plots of normalized HRR with normalized [OH][CH_2O] and [H][CH_2O] for three regimes, AB, BC and CD, shown in Fig. 7 for E_{ig} = 0.13 mJ.

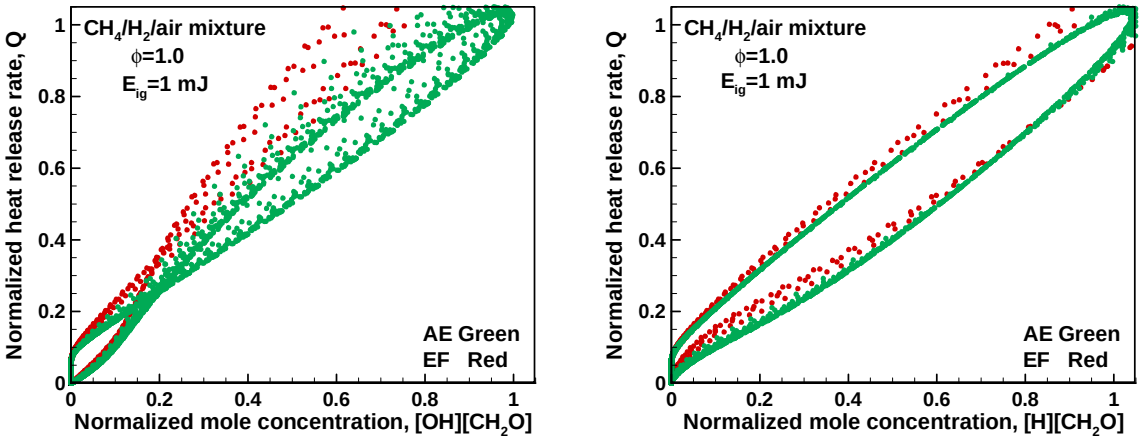

Figure 10. Scatter plots of normalized HRR against normalized [OH][CH_2O] and

[H][CH_2O] combinations for two regimes, AE and EF, shown in Fig. 7 for E_{ig} = 1.0 mJ.

To quantify the performance of the HRR markers at different stretch rates and ignition energies, we plot the correlation coefficient as a function of stretch rate for two ignition energies in Fig. 11. At a low ignition energy of E_{ig} = 0.13 mJ, the change of correlation coefficient follows the same trend as the *Sb*-K plot shown in Fig. 7 and exhibits three distinct regimes. It is noticed that although [OH][CH_2O] cannot quantitatively predict the HRR magnitude, it always shows a better quality in spatial reconstruction than [H][CH_2O].

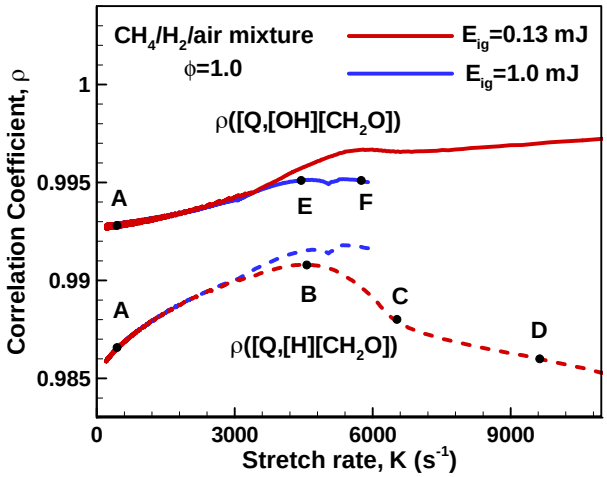

Figure 11. Change of the correlation coefficient with stretch rate during the ignition and propagation of SEF in a stoichiometric CH_4/H_2/air mixture with a=0.5 (i.e., CH_4:H_2=1:1) and with E_{ig} = 0.13 and 1.0 mJ.

Finally, the effect of H_2 addition on the spatial correlation of HRR with species molar concentrations is systematically analyzed for unstretched, adiabatic, planar flame in stoichiometric CH_4/H_2/air flames with different amounts of H_2 addition. The correlation coefficients are shown in Fig. 12. For a=0~0.7, H_2 addition is shown to be have little effect on the correlation coefficients. This indicates that the conventional HRR markers, [OH][CH_2O] and [H][CH_2O], can still be used for CH_4/H_2/air flames with H_2 blending ratio up to 70%. However, the correlation coefficients decrease quickly for a>0.7. This is reasonable since

hydrogen chemistry dominates the HRR when the binary fuel mainly consists of hydrogen. Note that in Fig. 12, the correlation coefficient is plotted against the volume fraction of hydrogen in the methane/hydrogen binary fuel blends. If the mass fraction is used instead, the curves and their trends will change substantially.

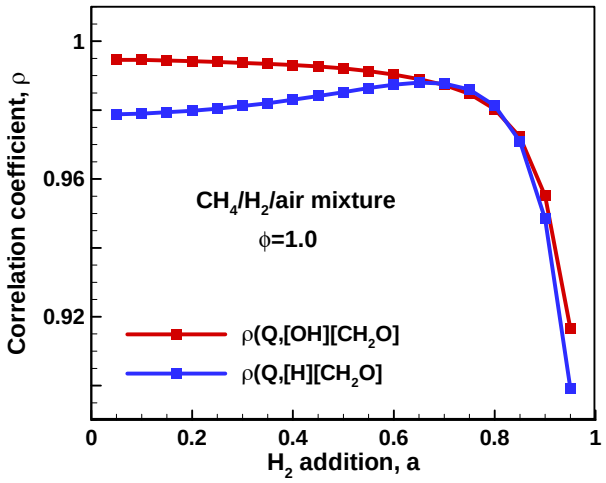

Figure 12. Change of the correlation coefficient with the amount H_2 addition in a stoichiometric unstretched planar CH_4/H_2/air flame. Here *a* is the volume fraction of H_2 in the CH_4/H_2 binary fuel blends.

3.3 Negatively-stretched Bunsen flames in CH_4/air and CH_4/H_2/air mixtures

Positively stretched flames are considered in the previous two subsections. For combustion processes in practical engines, the flame front is subjected to a wide range of stretch conditions including both positive and negative stretch rates. Therefore, in this subsection we consider Bunsen flames which have negative stretch rate at the flame tips.

Figure 13 shows the results for a steady cylindrical Bunsen flame in a stoichiometric CH_4/H_2/air mixture with a=0.5 (i.e., CH_4:H_2=1:1). Due to the non-uniform inlet flow which has a parabolic velocity profile, the flame front is shown to be curved especially for the regions around the flame tip and close to the base. Figure 13(c) shows the flame tip is highly-stretched and the stretch rate can reach -30000 s^{-1}. Since the mixture has a positive Markstein length as

indicated by Fig. 7, the combustion around the flame tip is enhanced by the negative stretch rate, and it has the highest HRR as shown by Fig. 13(b). Similar results are obtained for CH_4/air mixtures without H_2 addition but not presented here.

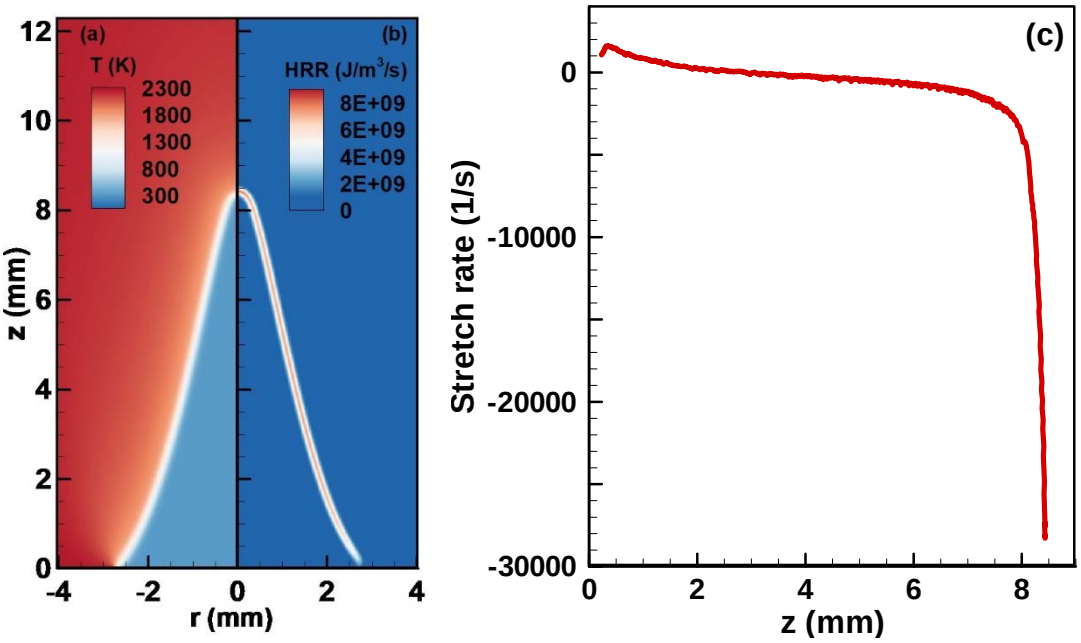

Figure 13. The results for 2D steady cylindrical Bunsen-type flame in a stoichiometric CH_4/H_2/air mixture with a=0.5 (i.e., CH_4:H_2=1:1): (a) temperature distribution, (b) HRR distribution, and (c) the flame stretch rate distribution around the flame tip.

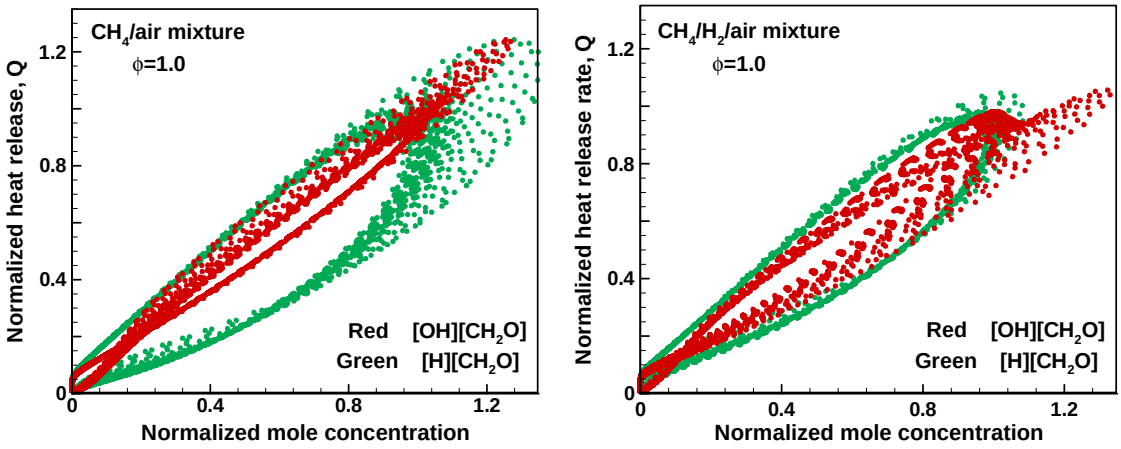

Figure 14. Scatter plots of normalized HRR against normalized [OH][CH_2O] and [H][CH_2O] for Bunsen flames in stoichiometric CH_4/air and CH_4/H_2/air (a=0.5) mixtures.

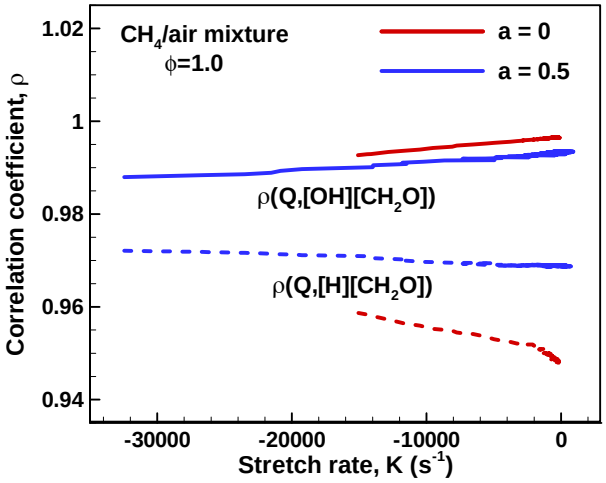

Figure 17. Change of the correlation coefficient with stretch rate for Bunsen flames in stoichiometric CH_4/air and CH_4/H_2/air (a=0.5) mixtures.

Then we examine the correlation between HRR and species concentrations for Bunsen flame with negative stretch rate. CH_4/air mixtures without and with H_2 addition are both considered. Figure 14 shows the scatter plots of normalized HRR against normalized $[OH][CH_2O]$ and $[H][CH_2O]$. These scatters are extracted from around 200 sample lines along the normal direction of the negatively-stretched flame tips. The change of correlation coefficient with local stretch rate is also shown in Fig. 15. The results indicate that both $[OH][CH_2O]$ and $[H][CH_2O]$ correlate well with the HRR for CH_4/air and CH_4/H_2/air Bunsen flames with highly-negatively-stretched flame tips. Compared to $[H][CH_2O]$, $[OH][CH_2O]$ has a better linear correlation with HRR. H_2 addition slightly strengthens the linear correlation between $[H][CH_2O]$ and HRR, while it weakens the correlation between $[OH][CH_2O]$ and HRR. At a large negative stretch rate, the peak of normalized $[OH][CH_2O]$ is much higher than that of the normalized HRR. This trend is opposite to that for positively-stretched SEFs considered in the previous subsection. The scatters in Fig. 14 are similar to those for SEFs in the normal flame propagation regime as shown in Figs. 3, 4, 9 and 10. We also consider Bunsen flames in fuel-rich CH_4/air mixture with ϕ=1.3 and similar results are obtained. These results demonstrate the broad range

of stretch rate does not obviously affect the correlations between HRR and two markers, [OH][CH_2O] and [H][CH_2O].

4. Conclusions

One- and two-dimensional simulations considering detailed chemistry and transport are conducted to assess the performance of two heat release rate markers, [H][CH_2O] and [OH][CH_2O], for premixed CH_4/air flames without and with H_2 addition. Both positively-stretched SEF and negatively-stretched Bunsen flame are considered. It is found that both HRR markers can qualitatively describe the spatial distribution of HRR at different stretch conditions. Compared to [H][CH_2O], [OH][CH_2O] exhibits a slightly better behavior and it has a higher correlation coefficient and lower sensitivity to the equivalence ratio. During the ignition-influenced phase of SEF, the normalized molar concentrations are lower than their corresponding normalized HRR values. This indicates that the magnitude of HRR may not be accurately predicted by the absolute values of species molar concentrations. With hydrogen addition, the spatial performance of these two markers does not change greatly. The correlation coefficients of these two markers are insensitive to the hydrogen addition when its volume fraction in methane/hydrogen binary fuel blends is below 70%. The present results demonstrate that the conventional HRR markers, [OH][CH_2O] and [H][CH_2O], can still be used to quantify the shape of HRR profiles even for highly-stretched premixed flames with small amount of hydrogen addition. Nevertheless, the magnitude of HRR cannot be accurately correlated by these two HRR markers for highly-stretched ignition kernel and hydrogen-dominated binary fuel blends.

In this work, we consider the binary fuel blends of methane/hydrogen. In future works, it would be interesting to consider ammonia blended by methane, which has received great attention recently.[53]

Acknowledgements

This work was supported by National Natural Science Foundation of China (No. 51861135309). Z.C. thanks Prof. Gaofeng Wang at Zhejiang University for helpful discussion, which made us to consider methane/hydrogen binary fuel blends besides pure methane.

References

(1) Yin, Y.; Gong, X.; Zhou, H.; Ren, Z., The correlation of species concentration with heat release rate in an auto-igniting turbulent n-heptane spray flame. *Fuel* **2020,** 262, 116510.

(2) Mulla, I. A.; Dowlut, A.; Hussain, T.; Nikolaou, Z. M.; Chakravarthy, S. R.; Swaminathan, N.; Balachandran, R., Heat release rate estimation in laminar premixed flames using laser-induced fluorescence of CH_2O and H-atom. *Combust. Flame* **2016,** 165, 373-383.

(3) Najm, H. N.; Paul, P. H.; Mueller, C. J.; Wyckoff, P. S., On the Adequacy of Certain Experimental Observables as Measurements of Flame Burning Rate. *Combust. Flame* **1998,** 113, 312-332.

(4) Balachandran, R.; Ayoola, B. O.; Kaminski, C. F.; Dowling, A. P.; Mastorakos, E., Experimental investigation of the nonlinear response of turbulent premixed flames to imposed inlet velocity oscillations. *Combust. Flame* **2005,** 143 , 37-55.

(5) Kathrotia, T.; Riedel, U.; Warnatz, J. In *A Numerical Study on the Relation of OH*, CH*, and C2* Chemiluminescence and Heat Release in Premixed Methane Flames*, 4th European Combustion Meeting, 2009.

(6) Zhang, F.; Zirwes, T.; Nawroth, H.; Habisreuther, P.; Bockhorn, H.; Paschereit, O., Combustion-generated noise: an environment related issue for future combustion systems. *Energy Technology* **2017,** 5, 1045-1054.

(7) Najm, H. N.; Knio, O. M.; Paul, P. H.; Wyckoff, P. S., A Study of Flame Observables in Premixed Methane - Air Flames. *Combust. Sci. Technol.* **1998,** 140, 369-403.

(8) Paul, P. H.; Najm, H. N., Planar laser-induced fluorescence imaging of flame heat release rate. *Symposium (International) on Combustion* **1998,** 27, 43-50.

(9) Böckle, S.; Kazenwadel, J.; Kunzelmann, T.; Shin, D. I.; Wolfrum, J., Simultaneous single-shot laser-based imaging of formaldehyde, OH, and temperature in turbulent flames. *Proc. Combust. Inst.* **2000,** 28, 279-286.

(10) Chi, C.; Janiga, G.; Zähringer, K.; Thévenin, D., DNS study of the optimal heat release rate marker in premixed methane flames. *Proc. Combust. Inst.* **2019,** 37, 2363-2371.

(11) Gordon, R.; Masri, A.; Mastorakos, E., Heat release rate as represented by [OH] × [CH_2O] and its role in autoignition. *Combust. Theor. Model.* **2009,** 13, 645-670.

(12) Yuan, R.; Kariuki, J.; Dowlut, A.; Ba Lachandran, R.; Mastorakos, E., Reaction zone visualisation in swirling spray n-heptane flames. *Proc. Combust. Inst.* **2015,** 35, 1649-1656.

(13) Fayoux, A.; Zahringer, K.; Gicquel, O.; Rolon, J. C., Experimental and numerical determination of heat release in counterflow premixed laminar flames. *Proc. Combust. Inst.* **2005,** 30, 251-257.

(14) Wang, H.; Hawkes, E.; Zhou, B.; Chen, J.; Li, Z.; Alden, M., A comparison between direct numerical simulation and experiment of the turbulent burning velocity-related statistics in a turbulent methane-air premixed jet flame at Karlovitz number. *Proc. Combust. Inst.* **2017,** 36, 2045-2053.

(15) Nikolaou, Z. M.; Swaminathan, N., Heat release rate markers for premixed combustion. *Combust. Flame* **2014,** 161, 3073-3084.

(16) Lipatnikov, A. N.; Chomiak, J., Molecular transport effects on turbulent flame propagation and structure. *Prog. Energy Combust. Sci.* **2005,** 31, 1-73.

(17) Driscoll, J. F., Turbulent premixed combustion: Flamelet structure and its effect on turbulent burning velocities. *Prog. Energy Combust. Sci.* **2008,** 34, 91-134.

(18) Aspden, A. J.; Day, M. S.; Bell, J. B., Turbulence-chemistry interaction in lean premixed

hydrogen combustion. *Proc. Combust. Inst.* **2015,** 35, 1321-1329.

(19) Briones, A. M.; Aggarwal, S. K.; Katta, V. R., Effects of H_2 enrichment on the propagation characteristics of CH_4-air triple flames. *Combust. Flame* **2008,** 153, 367-383.

(20) Tang, C.; Zhang, Y.; Huang, Z., Progress in combustion investigations of hydrogen enriched hydrocarbons. *Renewable and Sustainable Energy Reviews* **2014,** 30, 195-216.

(21) Shrestha, S. O. B.; Karim, G. A., Hydrogen as an additive to methane for spark ignition engine applications. *Int. J. Hydrogen Energy* **1999,** 24, 577-586.

(22) Huang, Z.; Zhang, Y.; Zeng, K.; Liu, B.; Wang, Q., Measurements of laminar burning velocities for natural gas-hydrogen-air mixtures. *Combust. Flame* **2006,** 146, 302-311.

(23) Chen, Z., Effects of hydrogen addition on the propagation of spherical methane/air flames: A computational study. *Int. J. Hydrogen Energy* **2009,** 34, 6558-6567.

(24) Dai, P.; Chen, Z.; Chen, S., Ignition of methane with hydrogen and dimethyl ether addition. *Fuel* **2014,** 118, 1-8.

(25) Li, Z.; Han, W.; Liu, D.; Chen, Z., Laminar flame propagation and ignition properties of premixed iso-octane/air with hydrogen addition. *Fuel* **2015,** 158, 443-450.

(26) Mendez, L. D. A.; Tummers, M. J.; Veen, E. H. V.; Roekaerts, D. J. E. M., Effect of hydrogen addition on the structure of natural-gas jet-in-hot-coflow flames. *Proc. Combust. Inst.* **2015,** 35, 3557-3564.

(27) Li, Z.; Gou, X.; Chen, Z., Effects of hydrogen addition on non-premixed ignition of iso-octane by hot air in a diffusion layer. *Combust. Flame* **2019,** 199, 292-300.

(28) Chen, Z., On the accuracy of laminar flame speeds measured from outwardly propagating spherical flames: Methane/air at normal temperature and pressure. *Combust. Flame* **2015,** 162, 2442-2453.

(29) Faghih, M.; Chen, Z., The constant-volume propagating spherical flame method for laminar flame speed measurement. *Science Bulletin* **2016,** 61, 1296-1310.

(30) Konnov, A. A.; Mohammad, A.; Kishore, V. R.; Kim, N. I.; Prathap, C.; Kumar, S., A comprehensive review of measurements and data analysis of laminar burning velocities for various fuel+air mixtures. *Prog. Energy Combust. Sci.* **2018,** 168, 197-267.

(31) Chen, Z.; Burke, M. P.; Ju, Y., On the critical flame radius and minimum ignition energy for spherical flame initiation. *Proc. Combust. Inst.* **2011,** 33, 1219-1226.

(32) Chen, Z.; Burke, M. P.; Ju, Y., Effects of Lewis number and ignition energy on the determination of laminar flame speed using propagating spherical flames. *Proc. Combust. Inst.* **2009,** 32, 1253-1260.

(33) Wang, Y.; Han, W.; Chen, Z., Effects of fuel stratifcation on ignition kernel development and minimum ignition energy of n-decane/air mixtures. *Proc. Combust. Inst.* **2019,** 37, 1623-1630.

(34) Mahdi, F.; Li, H.; Gou, X.; Chen, Z., On laminar premixed flame propagating into autoigniting mixtures under engine-relevant conditions. *Proc. Combust. Inst.* **2019,** 37, 4673-4680.

(35) Wang, Y.; Jayachandran, J.; Chen, Z., Effects of pressure rise rate on laminar flame speed under normal and engine-relevant conditions. *Combust. Theor. Model.* **2020,** 24, 953-964.

(36) Chen, X.; Zhao, P.; Dai, P.; Chen, Z., On the prediction of hot spot induced ignition by the Livengood-Wu integral. *Proc. Combust. Inst.* **2020,** 38, 4709-4716.

(37) Chen, X.; Bottler, H.; Scholtissek, A.; Hasse, C.; Chen, Z., Effects of stretch-chemistry interaction on chemical pathways for strained and curved hydrogen/air premixed flames. *Combust. Flame* **2021,** 232, 111532.

(38) Zhang, W.; Chen, Z.; Kong, W., Effects of diluents on the ignition of premixed H_2/air mixtures. *Combust. Flame* **2012,** 159, 151-160.

(39) Santner, J.; Haas, F. M.; Ju, Y.; Dryer, F. L., Uncertainties in interpretation of high pressure spherical flame propagation rates due to thermal radiation. *Combust. Flame* **2014,** 161, 147-

153.

(40) Yu, H.; Han, W.; Santner, J.; Gou, X.; Sohn, C. H.; Ju, Y.; Chen, Z., Radiation-induced uncertainty in laminar flame speed measured from propagating spherical flames. *Combust. Flame* **2014,** 161, 2815-2824.

(41) Chen, Z., Effects of radiation absorption on spherical flame propagation and radiation-induced uncertainty in laminar flame speed measurement. *Proc. Combust. Inst.* **2017,** 36, 1129-1136.

(42) Law, C. K., *Combustion Physics*. Cambridge University Press: 2006.

(43) Zirwes, T.; Zhang, F.; Habisreuther, P.; Hansinger, M.; Bockhorn, H.; Pfitzner, M.; Trimis, D., Quasi-DNS Dataset of a Piloted Flame with Inhomogeneous Inlet Conditions. *Flow, Turbulence and Combustion* **2020,** 104, 997-1027.

(44) Zirwes, T.; Zhang, F.; Denev, J. A.; Habisreuther, P.; Bockhorn, H., *Automated Code Generation for Maximizing Performance of Detailed Chemistry Calculations in OpenFOAM*. High Performance Computing in Science and Engineering ' 17: 2018.

(45) Goodwin, D. G., Cantera C++ User's Guide. *California Institute of Technology* **2002**.

(46) Wang, Y.; Zhang, H.; Zirwes, T.; Zhang, F.; Bockhorn, H.; Chen, Z., Ignition of dimethyl ether/air mixtures by hot particles: Impact of low temperature chemical reactions. *Proc. Combust. Inst.* **2021,** 38, 2459-2466.

(47) Zirwes, T.; Zhang, F.; Habisreuther, P.; Hansinger, M.; Bockhorn, H.; Pfitzner, M.; Trimis, D., Identification of Flame Regimes in Partially Premixed Combustion from a Quasi-DNS Dataset. *Flow, Turbulence and Combustion* **2021,** 106, 373-404.

(48) Zirwes, T.; Häber, T.; Zhang, F.; Kosaka, H.; Dreizler, A.; Steinhausen, M.; Hasse, C.; Stagni, A.; Trimis, D.; Suntz, R.; Bockhorn, H., Numerical Study of Quenching Distances for Side-Wall Quenching Using Detailed Diffusion and Chemistry. *Flow, Turbulence and Combustion* **2021,** 106, 649-679.

(49) Zirwes, T.; Zhang, F. C.; Wang, Y. Q.; Habisreuther, P.; Denev, J. A.; Chen, Z.; Bockhorn, H.; Trimis, D., In-situ flame particle tracking based on barycentric coordinates for studying local flame dynamics in pulsating Bunsen flames. *Proc. Combust. Inst.* **2021**, 38, 2057-2066.

(50) Smith, G.; Golden, D. M.; Frenklach, M.; Moriarty, N. W.; Eiteneer, B.; Goldenberg, M.; Bowman, C. T.; Hanson, R. K.; Song, S.; Gardiner, W. C.; Jr.; Lissianski, V. V.; Qin, Z., The GRI-Mech 3.0 chemical kinetic mechanism. *http://www.me.berkeley.edu/gri_mech/*.

(51) Wang, Y.; Movaghar, A.; Wang, Z.; Liu, Z.; Sun, W.; Egolfopoulos, F. N.; Chen, Z., Laminar flame speeds of methane/air mixtures at engine conditions: Performance of different kinetic models and power-law correlations. *Combust. Flame* **2020,** 218, 101-108.

(52) Kee, R. J.; Grcar, J. F.; Smooke, M. D., A FORTRAN Program for Modeling Steady Laminar One-Dimensional Premixed Flames. *Sandia National Laboratories Report SAND* **1985**, 85-8240.

(53) Valera-Medina, A.; Amer-Hatem, F.; Azad, A. K.; Dedoussi, I. C.; de Joannon, M.; Fernandes, R. X.; Glarborg, P.; Hashemi, H.; He, X.; Mashruk, S.; McGowan, J.; Mounaim-Rouselle, C.; Ortiz-Prado, A.; Ortiz-Valera, A.; Rossetti, I.; Shu, B.; Yehia, M.; Xiao, H.; Costa., M., Review on Ammonia as a Potential Fuel: From Synthesis to Economics. *Energy & Fuels* **2021**, 35, 6964−7029.